ARTICLE

2D V_2C MXene/ 2D g-C_3N_4 nanosheet heterojunctions constructed via - one-pot method for remedying water pollution through high-efficient adsorption cooperated with in-situ photocatalytic degradation

Received 00th January 20xx,
Accepted 00th January 20xx

DOI: 10.1039/x0xx00000x

Shishan Xue,*[a] Dengliang He,*[a] Herong Zhang,[a] Yuning Zhang,[a] Yu Wang,[a] Yurong Zeng,[a] Shuxin Liu,[a] Ning Chen[a]

Experimental Section

Materials

Urea (AR≥99%) and hydrofluoric acid (HF, 49%) were purchased from Shanghai Macklin Biochemical Co., Ltd. to synthesis the graphitic carbon nitride (g-C_3N_4). V_2AlC Max (≥99%) was purchased from Jinzhou Haixin Metal Materials Co., Ltd. as the precursor to prepare V_2C MXene. Rhodamine B (RhB), crystal violet (CV), methylene blue (MB) were obtained from Fuchen (Tianjin) Chemical Reagent Co., LTD. Hydrochloric acid (HCl, 37%) and sodium hydroxide (NaOH, AR) were acquired from Merck & Co. Inc. All the chemicals were used directly without refinement. Deionized water was used throughout the experiment.

Synthesis of bulk g-C_3N_4

The thermal polycondensation approach was carried out to synthesis g-C_3N_4 using urea as precursor.[1,] 2Urea (10.0 g) was placed in a corundum crucible with lid and heated in muffle furnace at 550 ℃ with the heating rate of 10 ℃/min for 2 h in air atmosphere. The fine faint yellow powder was the as-prepared bulk g-C_3N_4 which was preserved in sealed vessels for following fabrication of heterojunction.

Synthesis of V_2C MXene

The V_2C MXene nanosheets was obtained by etching V_2AlC Max with HF solution in Teflon tank to remove Al layer.[3] Firstly, V_2AlC Max (1.0 g) was added to HF (20 mL) in Teflon tank magnetically stirred for different etching time (12 h, 24 h, 48 h) at room temperature. Then, all the V_2C MXene suspensions were centrifuged to gather the powder and washed by deionized water until the pH value of the supernatant reached ~6 (Scheme 1a). The best etching time of V_2C MXene was 48 h. Finally, the product was freezing-dried for 3 days to obtain V_2C MXene nanosheets.

Synthesis of 2D/2D V_2C MXene/g-C_3N_4 nanosheet heterojunctions

The novel and simple strategy of one-pot simultaneously etching and self-assembling method was firstly employed to fabricate 2D/2D V_2C MXene/g-C_3N_4 nanosheet composite. The best synthesis route of V_2C MXene was ascertained in the previous etching step which was employed in this procedure to construct the 2D/2D V_2C MXene/g-C_3N_4 nanosheet heterojunction (2D/2D V_2C/g-C_3N_4 heterojunction). Briefly, V_2AlC Max and the obtained bulk g-C_3N_4 was added in the HF solution (20 mL) with different mass ratio (V_2AlC: g-C_3N_4=2:1, 1:1, 1:2, 1:5, 1:7) in Teflon tank magnetically stirred for 48 h at room temperature. During the procedure, the Al layer of V_2AlC Max was removed to get V_2C MXene and the bulk g-C_3N_4 was etching exfoliated to g-C_3N_4 nanosheets. Meanwhile, V_2C MXene and g-C_3N_4 nanosheets self-assembled to receive the 2D/2D V_2C/g-C_3N_4 heterojunction. Subsequently, the suspensions were centrifuged and washed by deionized water until the pH value of the supernatant reached ~6 to gather the V_2C/g-C_3N_4 powder. Afterward, the final products were freezing-dried for 3 days to obtain 2D/2D V_2C/g-C_3N_4 heterojunction (Scheme 1b). The 2D/2D V_2C/g-C_3N_4 heterojunction were noted as V_xG_y, where V defined as V_2C MXene, G reflected as g-C_3N_4 nanosheets, x and y were the mass ratio of V_2AlC: g-C_3N_4 (2:1, 1:1, 1:2, 1:5, 1:7).

Characterization

The crystalline phase and structure of the composites were determined by X-ray diffraction (XRD, Rigaku Ultima IV) using Cu K_α radiation, λ=1.5406 Å with the scanning rate of 10°/min from 5° to 90°. Fourier Transform Infrared (FT-IR) spectroscopy (Nicolet 6700 FTIR) recorded the functional moieties of the composite hydrogel in the wavenumber range from 400-4000 cm^{-1}. The Raman analysis was performed by Raman spectroscopy (Renishaw-inVia) with laser emission wavelength of 532 nm. The X-ray photoelectron spectra (XPS) were

[a] Chemistry and Chemical Engineering School, Mianyang Teachers' College, Mianxing Road No. 166, Mianyang City, Sichuan Province, China. 621000. E-mail: xueshishancarol@163.com; 449011902@163.com

Supplementary Information available: [details of any supplementary information available should be included here]. See DOI: 10.1039/x0xx00000x

collected on Thermo Scientific ESCALAB Xi+ X-ray Photoelectron Spectrometer. Zeiss EVO MA15 scanning electronic microscope (SEM) was employed to observe the microstructure of the materials, while elemental composition was carried out using Energy Dispersive X-ray spectroscopy (EDX). Zeta Potential was performed by the dynamic light scattering measurement (Nano ZS, Malvern Instruments Ltd) at room temperature in the neutral environment. The specific surface area of the materials was calculated by N_2 adsorption-desorption isotherm data measured by Brunauer-Emmett-Teller (BET) analysis conducted with a surface area analyzer (Quantachrome Instruments v10.0). Photoluminescence (PL, Dual-FL) was carried out to investigate the effects of rate of recombination of the 2D/2D V_2C/g-C_3N_4 heterojunction. The light adsorption and gap were estimated by diffuse reflectance spectra (DRS, UV-3600Plus) in the ultraviolet-visible (UV-vis) range. Electrochemical experiments were made with 0.1 M Na_2SO_4 or 0.5M KCl in an electrode system consisting of Pt wire, Ag/AgCl electrode, and sample electrode (reference electrode) using an electrochemical workstation (CHI 660D) under dark environment or visible light environment.

Adsorption Test

The different amounts of dye contaminants (RhB, CV, MB) were dissolved in the deionized water with different pH value (4, 7, or 10) regulated by HCl or NaOH to obtain the dye solution with the concentration of 15, 20, or 25 mg/L. The V_xG_y (0.1 g) was added to the different dye solutions (100 mL) under dark environment. The concentrations of the dye solutions at different time were calculated by a predetermined calibration curve versus dye concentrations of a standard solution which were surveyed by UV-Visible spectrophotometry (PerkinElmer, model Lambda 650, Shelton, Connecticut, U.S.A) at λ_{max} (RhB for 554 nm, CV for 584 nm and MB for 660 nm). The adsorption rate was calculated by the following formula:

$$AR = \frac{C_0 - C_t}{C_0} \times 100\% \quad \text{(E-1)}$$

where C_o is the original concentration of the dye solutions, C_t is the concentration of the solution after the adsorption by V_xG_y at different times.

Kinetics of dyes adsorption on 2D/2D V_2C/g-C_3N_4 heterojunction

The adsorption experiments in different dye solutions were executed to evaluate the adsorption kinetics. The adsorption capacity of obtained V_xG_y for RhB, CV or MB at equilibrium (Q_e, mg/g) and different time intervals (Q_t, mg/g) were calculated via the following equations:

$$Q_e = \frac{(C_0 - C_e) \times V}{m} \quad \text{(E-2)}$$

$$Q_t = \frac{(C_0 - C_t) \times V}{m} \quad \text{(E-3)}$$

Where, C_0 (mg/L) is the initial concentration of RhB, CV or MB solutions, C_e (mg/L) and C_t (mg/L) are the concentration of RhB, CV or MB solutions at equilibrium and a given time t, respectively. V (L) is the volume of RhB, CV or MB solutions and m (g) represents the weight of obtained V_xG_y.

The adsorption behavior of as-prepared V_xG_y for RhB, CV or MB was investigated through pseudo-first-order kinetic model, pseudo-second-order kinetic model and intraparticle diffusion model, of which formulas were shown as follow:

$$\ln(Q_e - Q_t) = \ln Q_e - K_1 t \quad \text{(E-6)}$$

$$\frac{t}{Q_t} = \frac{1}{K_2 Q_e^2} + \frac{t}{Q_e} \quad \text{(E-7)}$$

$$Q_t = K_p t^{0.5} + C \quad \text{(E-8)}$$

Where K_1 (min^{-1}), K_2 (min^{-1}) and K_p (g/mg/min) was the adsorption rate constant of pseudo-first-order kinetic model, pseudo-second-order kinetic model and intraparticle diffusion model, respectively. C reflects a constant associated with the boundary layer. The implications of Q_e and Q_t were displayed in previous paragraph.

Photocatalysis Degradation Test

The photodegradation of dye pollutants (RhB, CV and MB with the different original concentrations of 15, 20 and 25 mg/L at different pH values of 4, 7 and 10) was researched using by V_xG_y composites which were beforehand put in the dye solution for 50 min in dark environment under magnetic stirring at room temperature to exclude the influence of adsorption. The light with full spectrum to visible light was supplied by metal halide lamp (50 W). The dye solutions equipping with V_xG_y composites in the beaker were placed between two lamps from which were at the distance of 20 cm (the intensity of light irradiation was controlled at 100 W/m^2). The solutions underwent the photodegradation procedure were measured by UV-vis spectrophotometry (PerkinElmer, model Lambda 650, Shelton, Connecticut, U.S.A) at λ_{max} (RhB for 554 nm, CV for 584 nm and MB for 660 nm). The photodegradation ratio was calculated by the equation:

$$DR = \frac{C_0 - C_t}{C_0} \times 100\% \quad \text{(E-9)}$$

where C_o is the concentration of the solution before illumination, C_t is the concentration of the solution after illumination.

Results

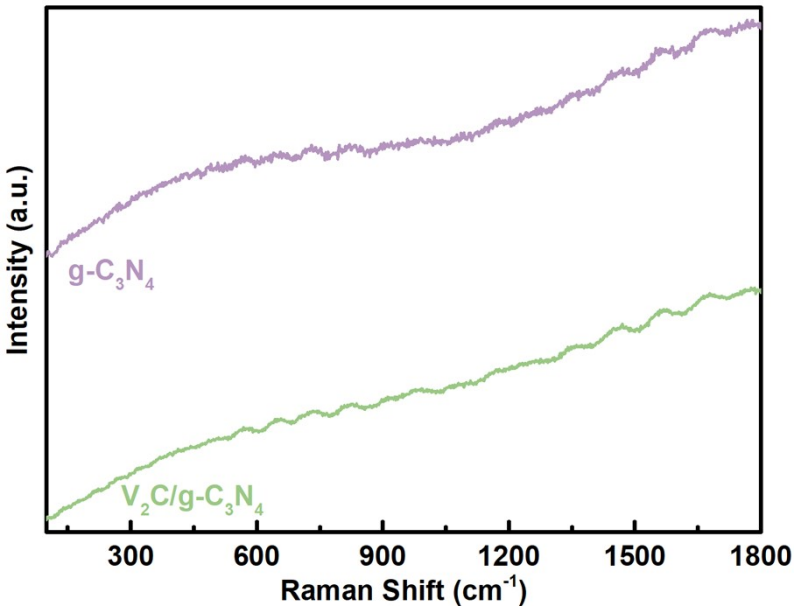

Fig. S1 Raman Spectra of bulk g-C_3N_4 and V_2C/g-C_3N_4 heterojunction.

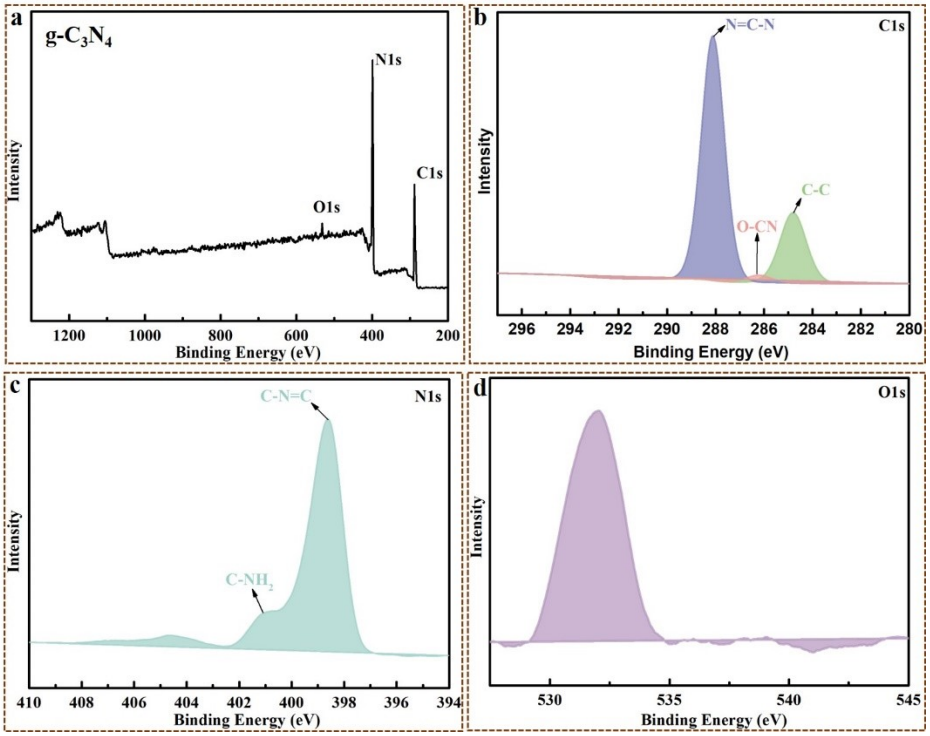

Fig. S2 The XPS spectra of (a) g-C_3N_4; (b) C 1s; (c) N 1s; (d) O 1s

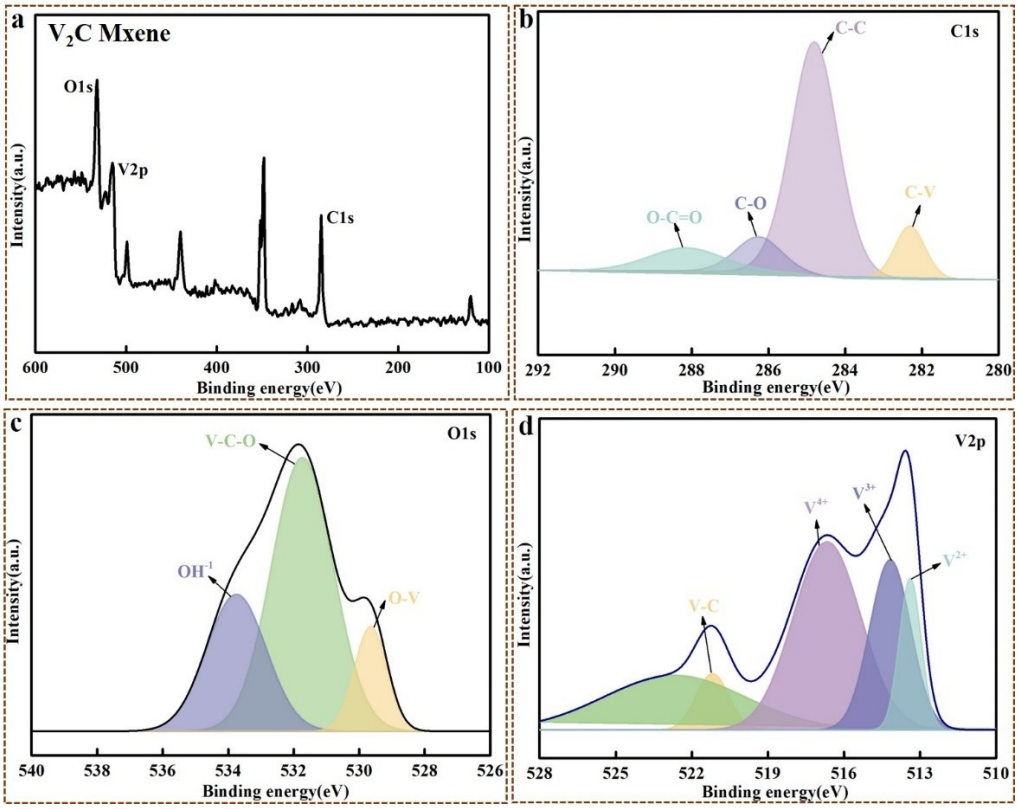

Fig. S3 The XPS spectra of (a) V_2C Mxene; (b) C 1s; (c) O 1s; (d) V 2p

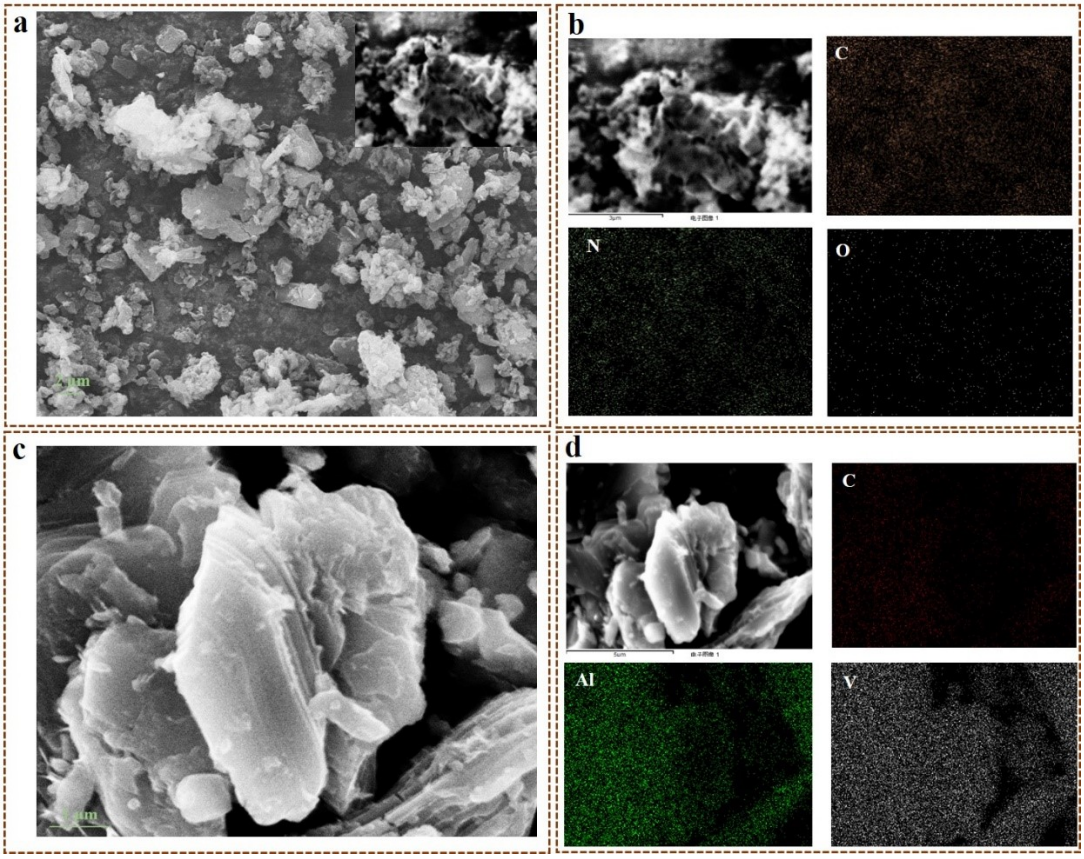

Fig. S4 (a) SEM image of bulk g-C_3N_4 (the insert image was g-C_3N_4 nanosheet) and (b) corresponding EDX mapping of bulk g-C_3N_4; (c) SEM image of V_2AlC and (d) corresponding EDX mapping of V_2AlC

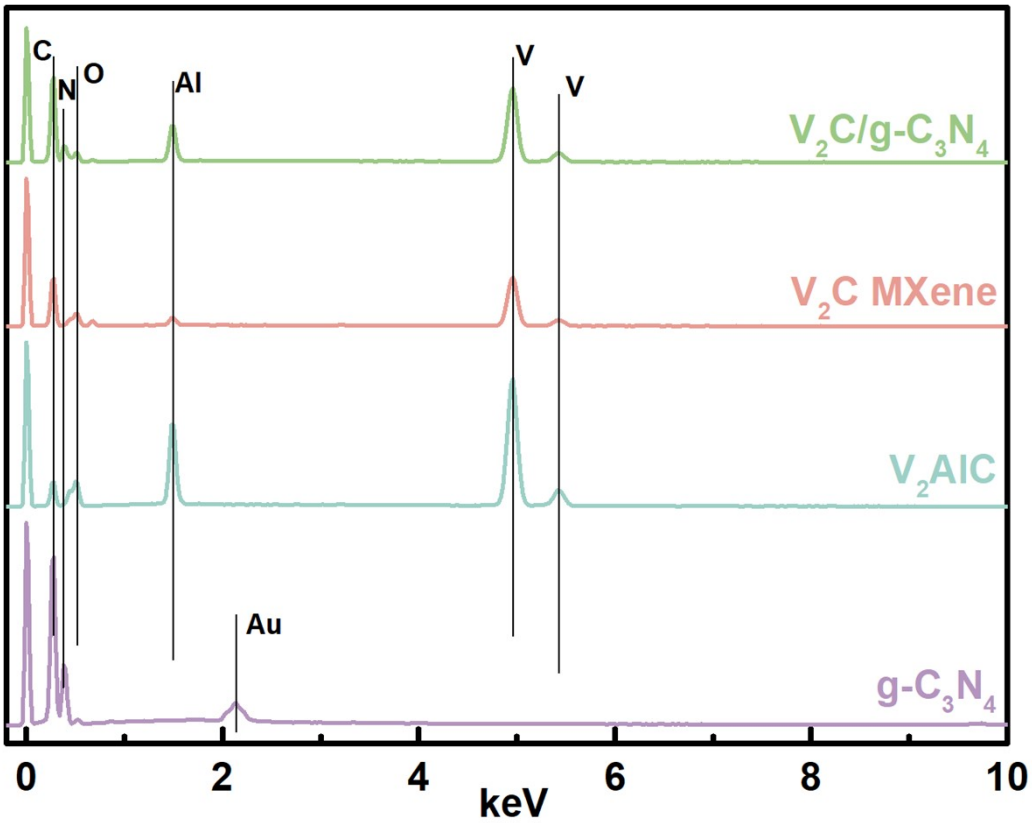

Fig. S5 EDX plots of g-C_3N_4, V_2AlC, V_2C MXene and V_2C/ g-C_3N_4 heterojunction

Table S1 The texture property of V_2AlC Max, V_2C Mxene, g-C_3N_4 and V_2C/g-C_3N_4 heterojunctions

Sample	S_{BET}(m^2/g)	V_p(cm^3/g)	Pore Diameter (nm)
V_2AlC Max	0.102	0.015	10.86
V_2C Mxene	7.135	0.063	13.94
g-C_3N_4	115.636	0.47	9.09
V_2C/g-C_3N_4	70.122	0.51	14.64

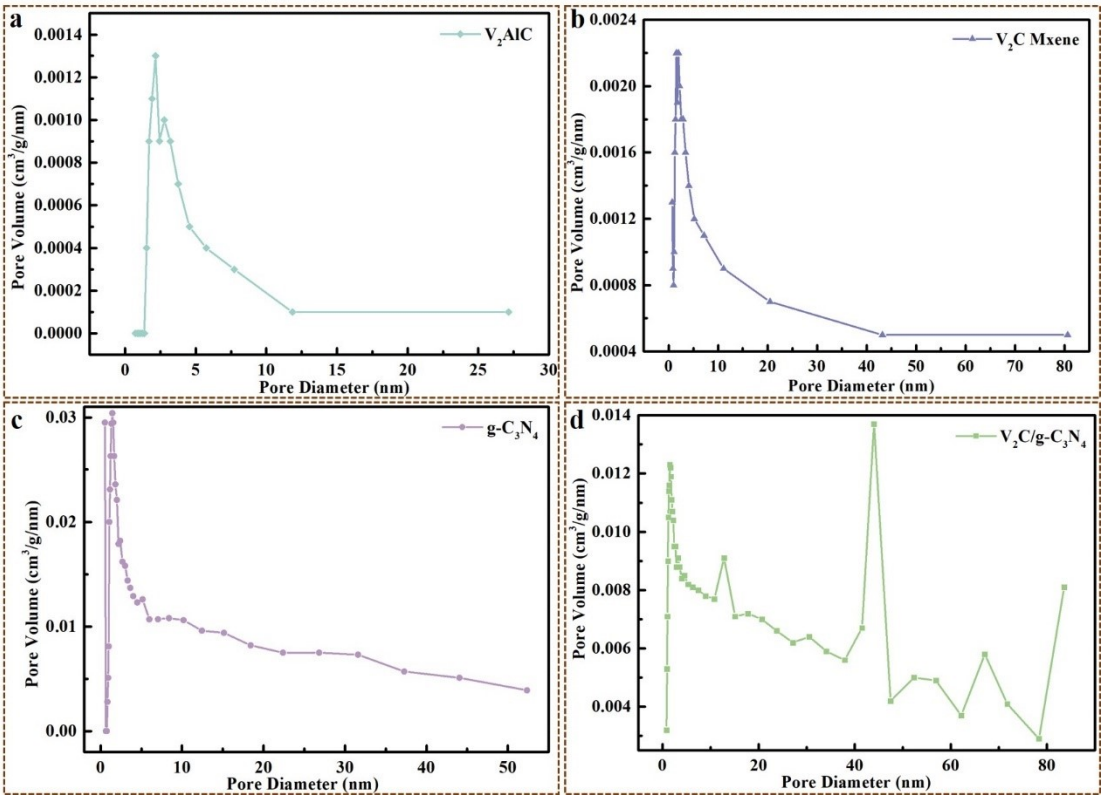

Fig. S6 BHJ pore size distribution of (a) V_2AlC Max, (b) V_2C Mxene, (c) g-C_3N_4 and (d) V_2C/g-C_3N_4 heterojunction

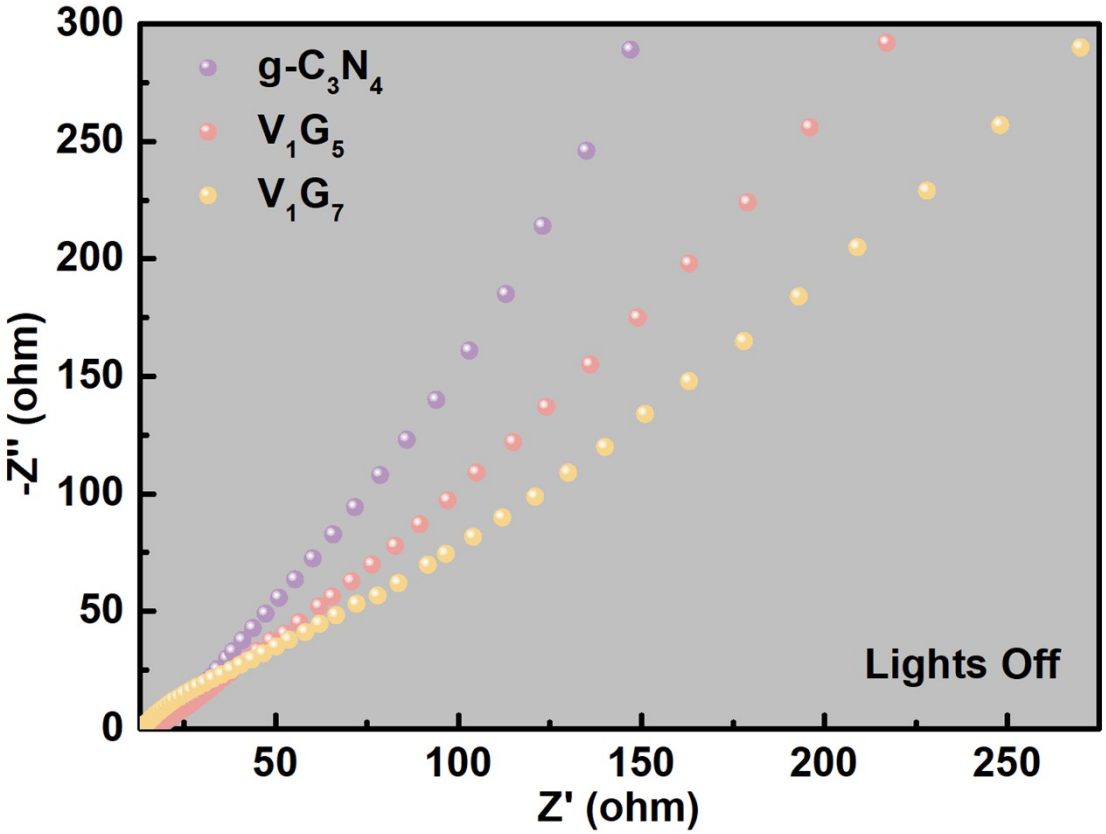

Fig. S7 Electrochemical impedance spectra (in the dark environment) of g-C_3N_4, V_1G_5 and V_1G_7 heterojunctions

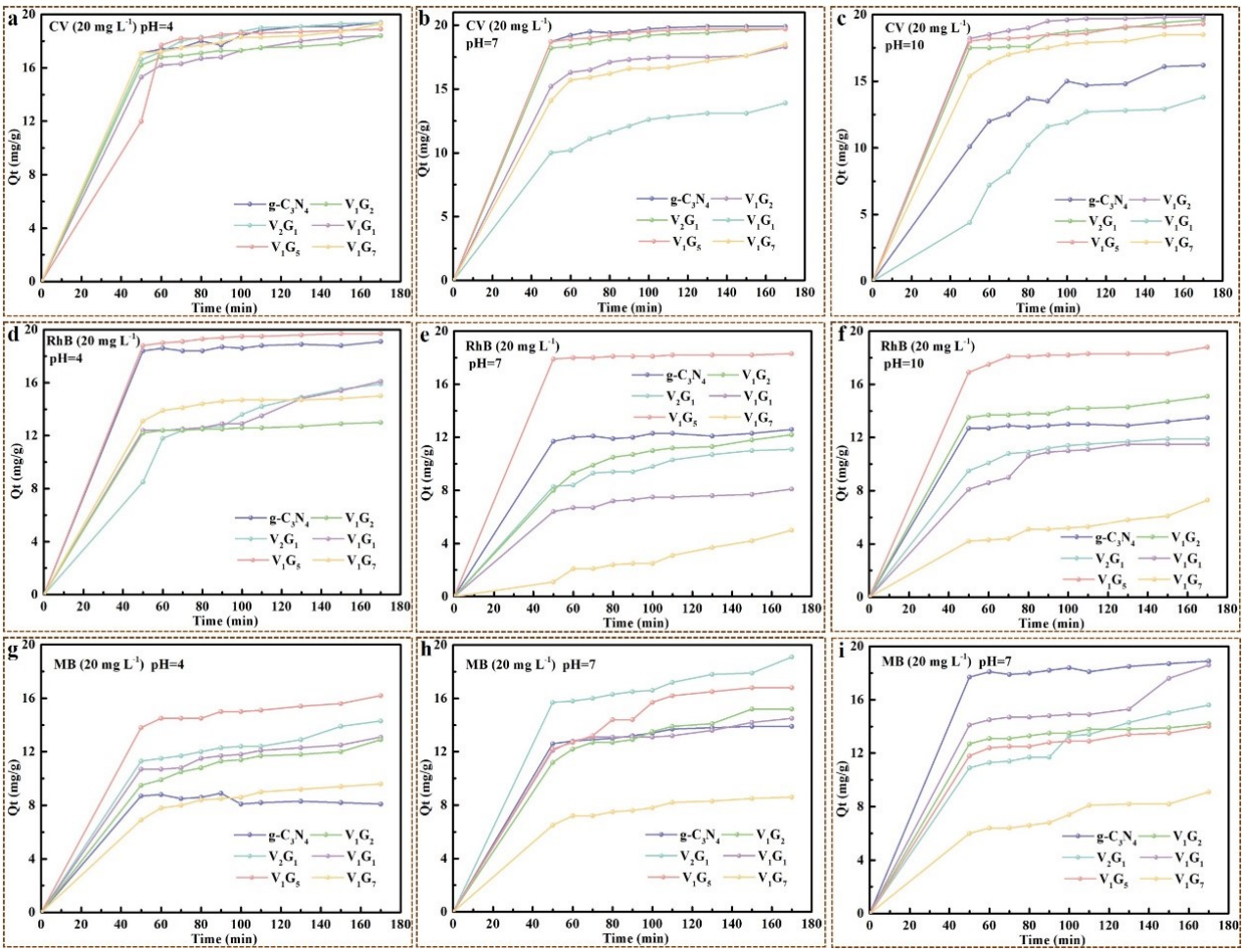

Fig. S8 Adsorption capacity (Q_t) of V_xG_y heterojunctions for CV (original content of 20 mg L^{-1}) at (a) pH=4, (b) pH=7, (c) pH=10; for RhB (original content of 20 mg L^{-1}) at (d) pH=4, (e) pH=7, (f) pH=10; for MB (original content of 20 mg L^{-1}) at (g) pH=4, (h) pH=7, (i) pH=10.

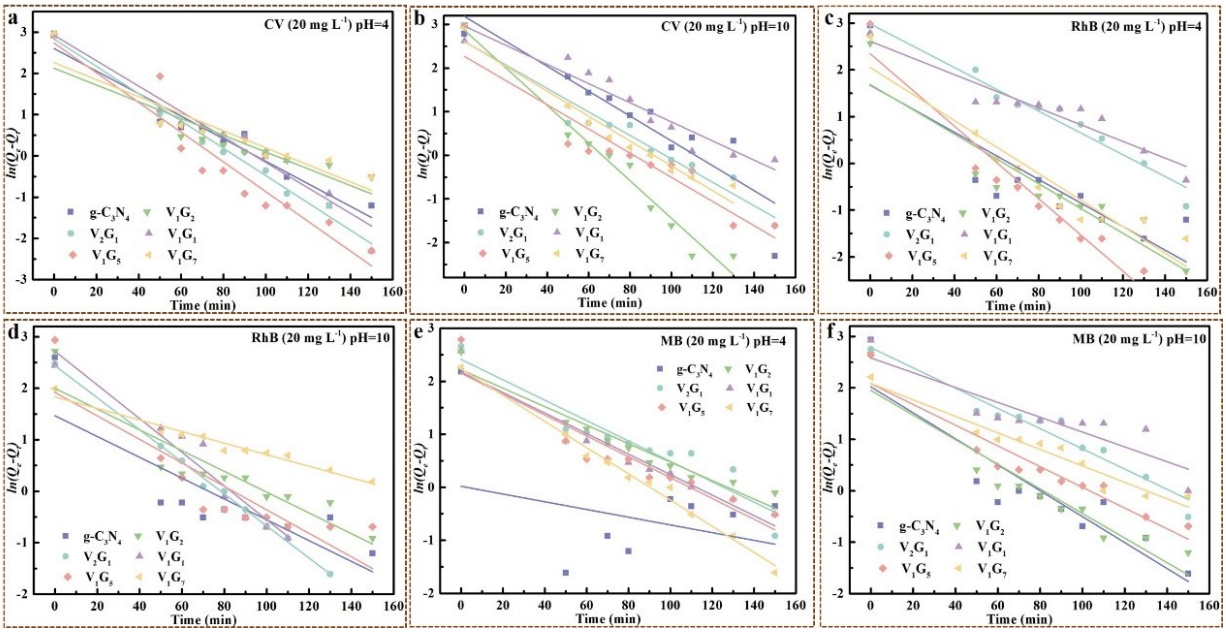

Fig. S9 Adsorption kinetics on the adsorption of CV at (a) pH=4, (b) pH=10; RhB at (c) pH=4, (d) pH=10; MB at (e) pH=4, (f) pH=10 with the original contents of 20 mg L^{-1} onto V_xG_y heterojunctions fitted by the pseudo-first-order kinetic model

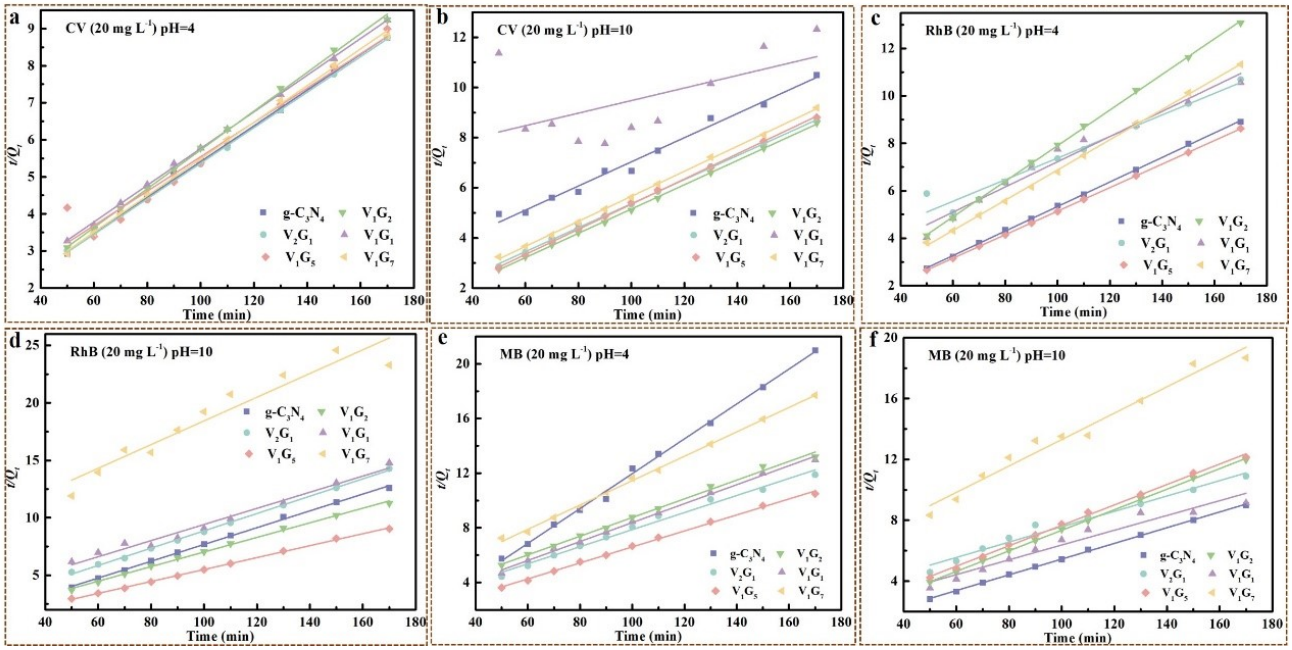

Fig. S10 Adsorption kinetics on the adsorption of CV (original content of 20 mg L^{-1}) at (a) pH=4, (b) pH=10; RhB (original content of 20 mg L^{-1}) at (c) pH=4, (d) pH=10; MB (original content of 20 mg L^{-1}) at (e) pH=4, (f) pH=10 onto V_xG_y heterojunctions fitted by the pseudo-second-order kinetic model

Table S2 kinetic parameters of CV by V_xG_y heterojunctions (pH=4, 20 mg L^{-1})

		Pseudo-first-order Kinetic Model				Pseudo-second-order Kinetic Model		
	C_0 (mg L^{-1})	$Q_{e,exp}$ (mg g^{-1})	$Q_{e,cal}$ (mg g^{-1})	K_1 (min^{-1})	R^2	$Q_{e,cal}$ (mg g^{-1})	K_2 (g mg^{-1} min^{-1})	R^2
g-C_3N_4	20	19.4	19.59	0.027	0.93897	19.52	0.048	0.99865
V_2G_1	20	19.4	19.47	0.033	0.98355	19.52	0.048	0.99956
V_1G_1	20	18.4	18.50	0.031	0.94266	18.52	0.050	0.99938
V_1G_2	20	18.4	19.04	0.020	0.81299	18.51	0.052	0.99863
V_1G_5	20	18.9	18.94	0.036	0.89978	19.03	0.046	0.95461
V_1G_7	20	19.3	19.86	0.021	0.84989	19.42	0.050	0.99855

Table S3 kinetic parameters of CV by V_xG_y heterojunctions (pH=7, 20 mg L^{-1})

		Pseudo-first-order Kinetic Model				Pseudo-second-order Kinetic Model		
	C_0 (mg L^{-1})	$Q_{e,exp}$ (mg g^{-1})	$Q_{e,cal}$ (mg g^{-1})	K_1 (min^{-1})	R^2	$Q_{e,cal}$ (mg g^{-1})	K_2 (g mg^{-1} min^{-1})	R^2
g-C_3N_4	20	19.9	20.10	0.027	0.93897	20.02	0.049	0.99985
V_2G_1	20	19.7	19.77	0.033	0.98355	19.82	0.049	0.99991
V_1G_1	20	13.9	13.97	0.031	0.94266	13.99	0.061	0.99551
V_1G_2	20	18.3	18.93	0.020	0.81299	18.41	0.052	0.99802
V_1G_5	20	19.7	19.74	0.036	0.89978	19.82	0.049	0.9999
V_1G_7	20	18.5	19.04	0.021	0.84989	18.62	0.049	0.99558

Table S4 kinetic parameters of CV by V_xG_y heterojunctions (pH=10, 20 mg L^{-1})

		Pseudo-first-order Kinetic Model				Pseudo-second-order Kinetic Model		
	C_0 (mg L^{-1})	$Q_{e,exp}$ (mg g^{-1})	$Q_{e,cal}$ (mg g^{-1})	K_1 (min^{-1})	R^2	$Q_{e,cal}$ (mg g^{-1})	K_2 (g mg^{-1} min^{-1})	R^2
g-C_3N_4	20	16.2	16.32	0.029	0.81275	16.32	0.048	0.98498
V_2G_1	20	19.6	19.80	0.027	0.935	19.72	0.048	0.99859
V_1G_1	20	13.8	14.13	0.022	0.90501	14.03	0.025	0.24713
V_1G_2	20	19.8	19.81	0.043	0.96602	19.92	0.048	0.99957
V_1G_5	20	19.3	19.47	0.028	0.87406	19.42	0.050	0.99939
V_1G_7	20	18.5	18.63	0.029	0.95732	18.62	0.050	0.99935

Table S5 kinetic parameters of RhB by V_xG_y heterojunctions (pH=4, 20 mg L^{-1})

		Pseudo-first-order Kinetic Model				Pseudo-second-order Kinetic Model		
	C_0 (mg L^{-1})	$Q_{e,exp}$ (mg g^{-1})	$Q_{e,cal}$ (mg g^{-1})	K_1 (min^{-1})	R^2	$Q_{e,cal}$ (mg g^{-1})	K_2 (g mg^{-1} min^{-1})	R^2

g-C_3N_4	20	19.1	19.38	0.025	0.68938	19.21	0.052	0.9996
V_2G_1	20	15.9	16.22	0.023	0.95019	16.03	0.046	0.96105
V_1G_1	20	16.1	16.89	0.018	0.88771	16.21	0.053	0.97009
V_1G_2	20	13	13.13	0.027	0.82867	13.08	0.075	0.99958
V_1G_5	20	19.7	19.73	0.039	0.93138	19.82	0.050	0.99998
V_1G_7	20	15	15.13	0.028	0.88404	15.09	0.064	0.99923

Table S6 kinetic parameters of RhB by V_xG_y heterojunctions (pH=7, 20 mg L^{-1})

		Pseudo-first-order Kinetic Model				Pseudo-second-order Kinetic Model		
	C_0 (mg L^{-1})	$Q_{e,exp}$ (mg g^{-1})	$Q_{e,cal}$ (mg g^{-1})	K_1 (min^{-1})	R^2	$Q_{e,cal}$ (mg g^{-1})	K_2 (g mg^{-1} min^{-1})	R^2
g-C_3N_4	20	12.6	12.96	0.021	0.6527	12.67	0.078	0.99854
V_2G_1	20	11.1	11.20	0.028	0.91449	11.18	0.075	0.99574
V_1G_1	20	8.1	8.43	0.019	0.91749	8.15	0.112	0.99687
V_1G_2	20	12.2	12.50	0.022	0.97868	12.29	0.068	0.99359
V_1G_5	20	18.3	18.39	0.031	0.73205	18.41	0.054	0.99997
V_1G_7	20	5	5.75	0.012	0.88355	4.60	-0.016	-0.1022

Table S7 kinetic parameters of RhB by V_xG_y heterojunctions (pH=10, 20 mg L^{-1})

		Pseudo-first-order Kinetic Model				Pseudo-second-order Kinetic Model		
	C_0 (mg L^{-1})	$Q_{e,exp}$ (mg g^{-1})	$Q_{e,cal}$ (mg g^{-1})	K_1 (min^{-1})	R^2	$Q_{e,cal}$ (mg g^{-1})	K_2 (g mg^{-1} min^{-1})	R^2
g-C_3N_4	20	13.5	13.97	0.020	0.65741	13.58	0.073	0.99847
V_2G_1	20	11.9	11.96	0.031	0.99629	11.98	0.075	0.99871
V_1G_1	20	11.5	11.54	0.033	0.92992	11.58	0.070	0.9796
V_1G_2	20	15.1	15.62	0.020	0.82096	15.19	0.064	0.9974
V_1G_5	20	18.8	19.18	0.023	0.72631	18.91	0.052	0.99903
V_1G_7	20	7.3	8.63	0.011	0.95697	7.36	0.103	0.91208

Table S8 kinetic parameters of MB by V_xG_y heterojunctions (pH=4, 20 mg L^{-1})

		Pseudo-first-order Kinetic Model				Pseudo-second-order Kinetic Model		
	C_0 (mg L^{-1})	$Q_{e,exp}$ (mg g^{-1})	$Q_{e,cal}$ (mg g^{-1})	K_1 (min^{-1})	R^2	$Q_{e,cal}$ (mg g^{-1})	K_2 (g mg^{-1} min^{-1})	R^2
g-C_3N_4	20	8.1	11.39	0.0073	-0.0628	8.30	0.128	0.9971
V_2G_1	20	14.3	14.89	0.019	0.87333	14.39	0.062	0.98784
V_1G_1	20	13.1	13.64	0.019	0.93378	13.18	0.069	0.9966
V_1G_2	20	12.9	13.66	0.017	0.93355	12.99	0.068	0.99476
V_1G_5	20	16.2	16.76	0.020	0.85924	16.30	0.059	0.99773
V_1G_7	20	9.6	9.74	0.025	0.9866	9.67	0.089	0.99826

Table S9 kinetic parameters of MB by V_xG_y heterojunctions (pH=7, 20 mg L^{-1})

		Pseudo-first-order Kinetic Model				Pseudo-second-order Kinetic Model		
	C_0 (mg L^{-1})	$Q_{e,exp}$ (mg g^{-1})	$Q_{e,cal}$ (mg g^{-1})	K_1 (min^{-1})	R^2	$Q_{e,cal}$ (mg g^{-1})	K_2 (g mg^{-1} min^{-1})	R^2
g-C_3N_4	20	13.9	13.94	0.035	0.94839	13.99	0.068	0.99947
V_2G_1	20	19.1	20.22	0.017	0.87692	19.22	0.048	0.99188
V_1G_1	20	14.5	14.92	0.021	0.85077	14.59	0.065	0.99489
V_1G_2	20	15.2	15.72	0.020	0.95328	15.30	0.056	0.99418
V_1G_5	20	16.8	16.90	0.030	0.93135	16.92	0.048	0.992
V_1G_7	20	8.6	8.67	0.028	0.96278	8.66	0.101	0.99816

Table S10 kinetic parameters of MB by V_xG_y heterojunctions (pH=10, 20 mg L^{-1})

		Pseudo-first-order Kinetic Model				Pseudo-second-order Kinetic Model		
	C_0 (mg L^{-1})	$Q_{e,exp}$ (mg g^{-1})	$Q_{e,cal}$ (mg g^{-1})	K_1 (min^{-1})	R^2	$Q_{e,cal}$ (mg g^{-1})	K_2 (g mg^{-1} min^{-1})	R^2
g-C_3N_4	20	18.9	19.17	0.025	0.80034	19.01	0.052	0.99921
V_2G_1	20	15.6	16.14	0.020	0.93686	15.71	0.051	0.97465
V_1G_1	20	18.6	20.50	0.014	0.76007	18.72	0.049	0.9471
V_1G_2	20	14.2	14.44	0.024	0.8747	14.29	0.068	0.99947
V_1G_5	20	14	14.48	0.020	0.88601	14.09	0.067	0.99756
V_1G_7	20	9.1	9.74	0.016	0.93286	9.17	0.087	0.9695

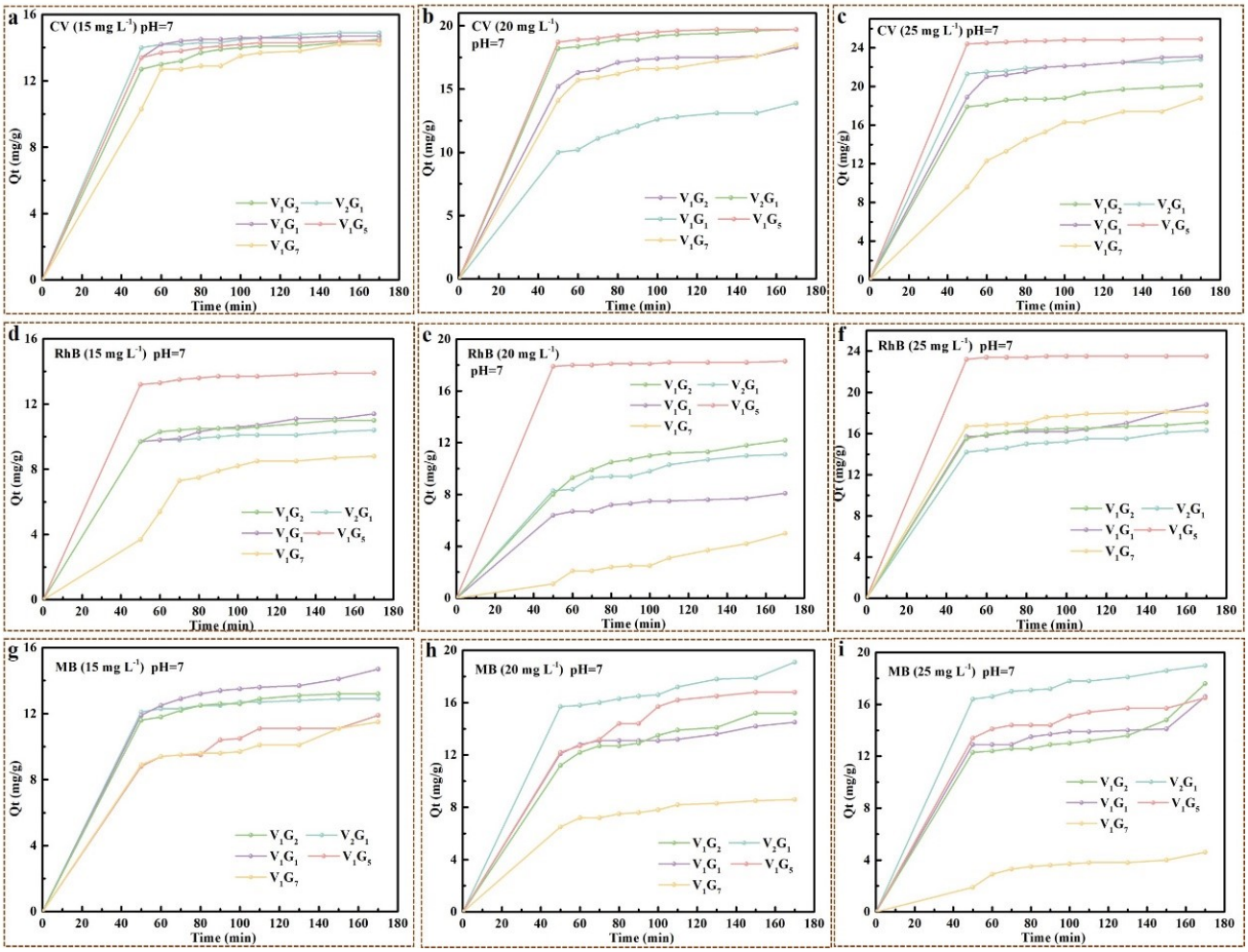

Fig. S11 Adsorption capacity (Q_t) of V_xG_y heterojunctions for CV (pH=7) with the original content of (a) 15 mg L^{-1}, (b) 20 mg L^{-1}, (c) 25 mg L^{-1}; for RhB (pH=7) with the original content of (d) 15 mg L^{-1}, (e) 20 mg L^{-1}, (f) 25 mg L^{-1}; for MB (pH=7) with the original content of (g) 15 mg L^{-1}, (h) 20 mg L^{-1}, (i) 25 mg L^{-1}.

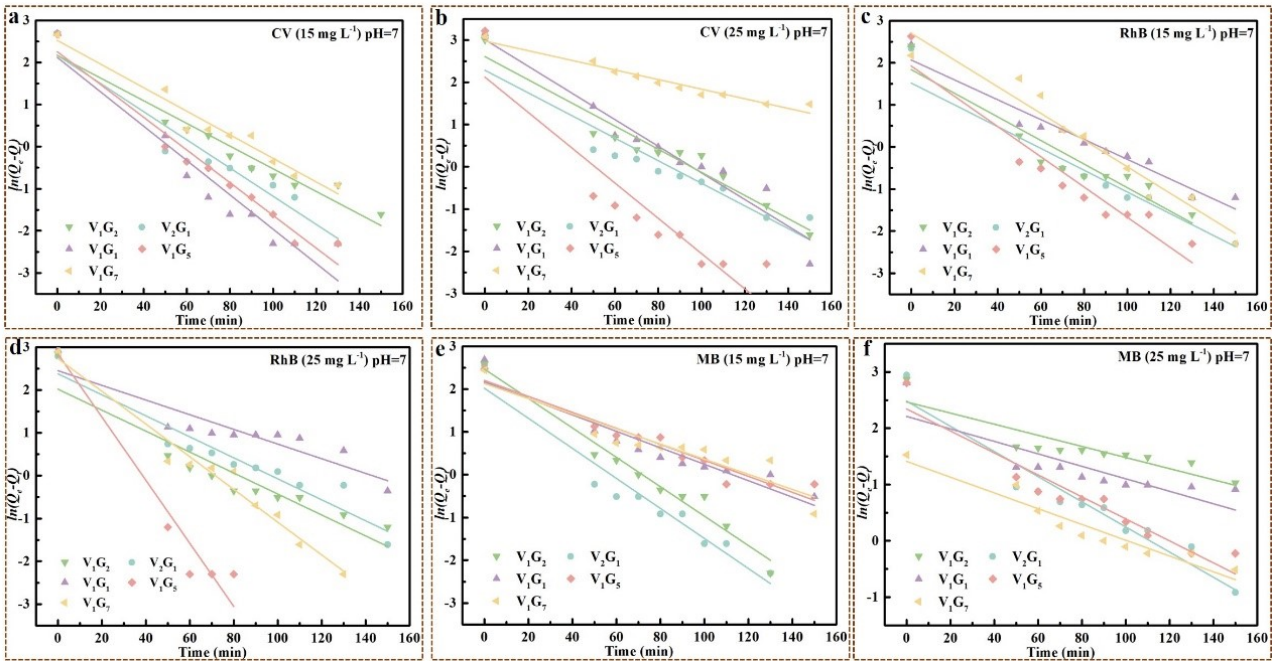

Fig. S12 Adsorption kinetics on the adsorption of CV with the original content of (a) 15 mg L^{-1}, (b) 25 mg L^{-1}; RhB with the original content of (c) 15 mg L^{-1}, (d) 25 mg L^{-1}; MB with the original content of (e) 15 mg L^{-1}, (f) 25 mg L^{-1} onto V_xG_y heterojunctions at pH value of 7 fitted by the pseudo-first-order kinetic model

Table S11 kinetic parameters of CV by V_xG_y heterojunctions (pH=7, 15 mg L^{-1})

		Pseudo-first-order Kinetic Model				Pseudo-second-order Kinetic Model		
	C_0 (mg L^{-1})	$Q_{e,exp}$ (mg g^{-1})	$Q_{e,cal}$ (mg g^{-1})	K_1 (min^{-1})	R^2	$Q_{e,cal}$ (mg g^{-1})	K_2 (g mg^{-1} min^{-1})	R^2
V_2G_1	15	14.9	14.95	0.03352	0.90111	14.99	0.06489	0.99971
V_1G_1	15	14.7	14.71	0.04083	0.90136	14.79	0.06615	0.99941
V_1G_2	15	14.5	14.65	0.02698	0.93453	14.59	0.06516	0.99955
V_1G_5	15	14.4	14.42	0.03891	0.95752	14.49	0.06721	0.9999
V_1G_7	15	14.2	14.32	0.02803	0.94933	14.29	0.0621	0.99245

Table S12 kinetic parameters of CV by V_xG_y heterojunctions (pH=7, 25 mg L^{-1})

		Pseudo-first-order Kinetic Model				Pseudo-second-order Kinetic Model		
	C_0 (mg L^{-1})	$Q_{e,exp}$ (mg g^{-1})	$Q_{e,cal}$ (mg g^{-1})	K_1 (min^{-1})	R^2	$Q_{e,cal}$ (mg g^{-1})	K_2 (g mg^{-1} min^{-1})	R^2
V_2G_1	25	22.8	23.04	0.02677	0.86549	22.94	0.04265	0.99982
V_1G_1	25	23.1	23.21	0.03156	0.93466	23.25	0.04013	0.99878
V_1G_2	25	20.1	20.29	0.0274	0.93502	20.22	0.04697	0.99903
V_1G_5	25	24.9	24.92	0.04179	0.8349	25.05	0.03981	0.99999
V_1G_7	25	18.8	21.97	0.01138	0.94981	18.96	0.03659	0.96075

Table S13 kinetic parameters of RhB by V_xG_y heterojunctions (pH=7, 15 mg L^{-1})

		Pseudo-first-order Kinetic Model				Pseudo-second-order Kinetic Model		
	C_0 (mg L^{-1})	$Q_{e,exp}$ (mg g^{-1})	$Q_{e,cal}$ (mg g^{-1})	K_1 (min^{-1})	R^2	$Q_{e,cal}$ (mg g^{-1})	K_2 (g mg^{-1} min^{-1})	R^2
V_2G_1	15	10.4	10.52	0.0259	0.84439	10.46	0.09351	0.99953
V_1G_1	15	11.4	11.61	0.02361	0.94714	11.47	0.08087	0.99887
V_1G_2	15	11	11.09	0.02807	0.88116	11.07	0.0866	0.99929
V_1G_5	15	13.9	13.93	0.03596	0.89928	13.98	0.07028	0.99995
V_1G_7	15	8.8	8.84	0.03173	0.9345	8.89	0.06726	0.69462

Table S14 kinetic parameters of RhB by V_xG_y heterojunctions (pH=7, 25 mg L^{-1})

		Pseudo-first-order Kinetic Model				Pseudo-second-order Kinetic Model		
	C_0 (mg L^{-1})	$Q_{e,exp}$ (mg g^{-1})	$Q_{e,cal}$ (mg g^{-1})	K_1 (min^{-1})	R^2	$Q_{e,cal}$ (mg g^{-1})	K_2 (g mg^{-1} min^{-1})	R^2
V_2G_1	25	16.3	16.56	0.02453	0.90353	16.40	0.0576	0.99856
V_1G_1	25	18.8	19.88	0.01714	0.8119	18.92	0.04955	0.98536
V_1G_2	25	17.1	17.37	0.02449	0.85089	17.20	0.05661	0.99967
V_1G_5	25	23.5	23.50	0.07374	0.92168	23.64	0.04237	0.99998
V_1G_7	25	18.1	18.13	0.03822	0.96475	18.21	0.0526	0.99945

Table S15 kinetic parameters of MB by V_xG_y heterojunctions (pH=7, 15 mg L^{-1})

		Pseudo-first-order Kinetic Model				Pseudo-second-order Kinetic Model		
	C_0 (mg L^{-1})	$Q_{e,exp}$ (mg g^{-1})	$Q_{e,cal}$ (mg g^{-1})	K_1 (min^{-1})	R^2	$Q_{e,cal}$ (mg g^{-1})	K_2 (g mg^{-1} min^{-1})	R^2
V_2G_1	15	12.9	12.93	0.03513	0.93206	12.98	0.07508	0.9999
V_1G_1	15	14.7	15.28	0.01924	0.89199	14.79	0.06331	0.9974
V_1G_2	15	13.2	13.24	0.03438	0.96514	13.28	0.07076	0.99965
V_1G_5	15	11.9	12.42	0.01869	0.91954	11.98	0.07309	0.99154
V_1G_7	15	11.5	12.10	0.01768	0.84378	11.57	0.07836	0.98159

Table S16 kinetic parameters of MB by V_xG_y heterojunctions (pH=7, 25 mg L^{-1})

		Pseudo-first-order Kinetic Model				Pseudo-second-order Kinetic Model		
	C_0 (mg L^{-1})	$Q_{e,exp}$ (mg g^{-1})	$Q_{e,cal}$ (mg g^{-1})	K_1 (min^{-1})	R^2	$Q_{e,cal}$ (mg g^{-1})	K_2 (g mg^{-1} min^{-1})	R^2
V_2G_1	25	19	19.44	0.02234	0.91727	19.12	0.04922	0.99823
V_1G_1	25	16.6	19.58	0.01108	0.68271	16.70	0.05817	0.96205
V_1G_2	25	17.6	21.64	0.00987	0.77785	17.71	0.05181	0.91061
V_1G_5	25	16.5	17.12	0.01953	0.90457	16.60	0.05587	0.99637
V_1G_7	25	18.4	20.28	0.014	0.91224	18.44	0.14472	0.81372

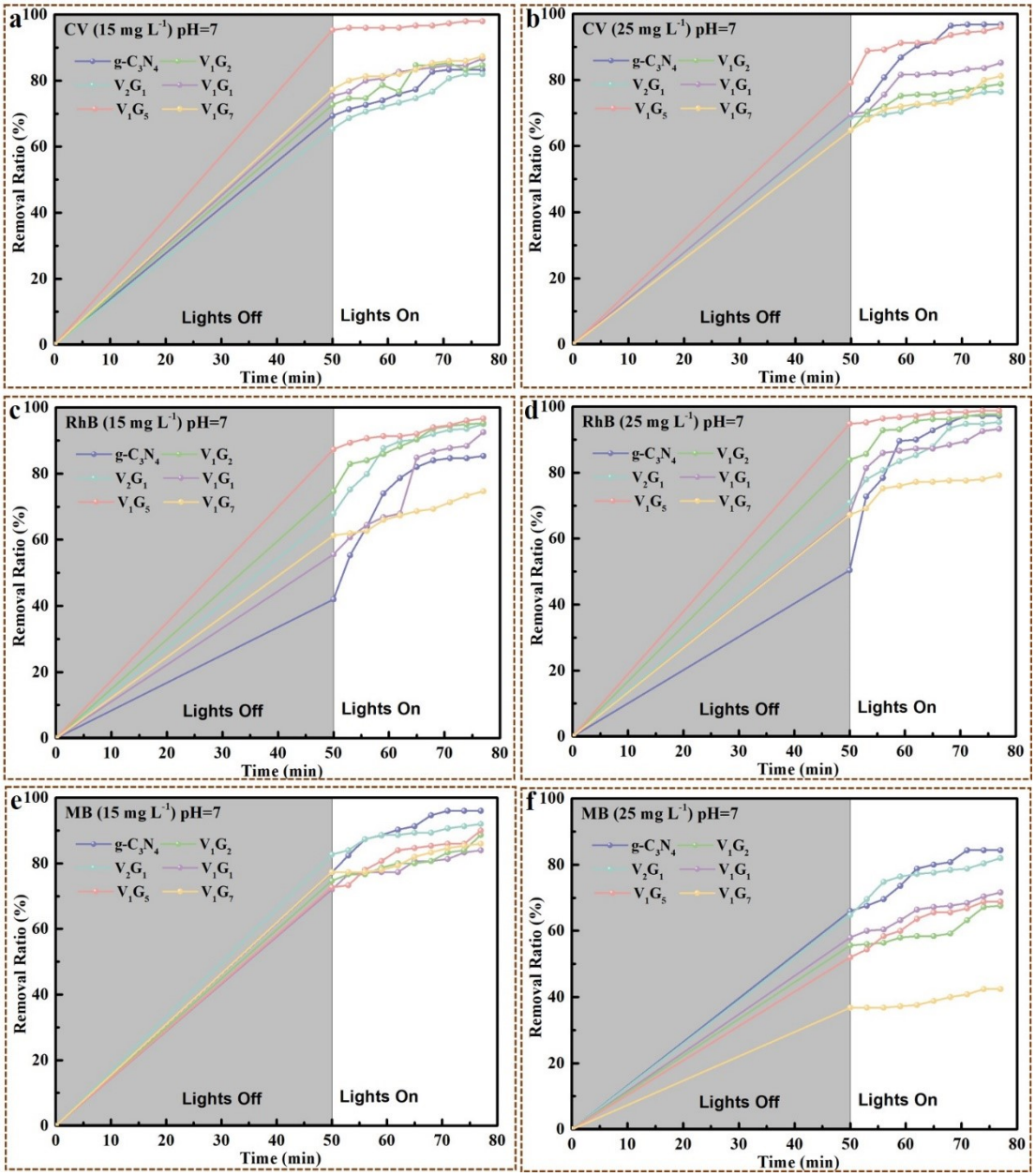

Fig. S13 Removal ratios of CV with the original content of (a) 15 mg L^{-1}, (b) 25 mg L^{-1}; RhB with the original content of (c) 15 mg L^{-1}, (d) 25 mg L^{-1}; MB with the original content of (e) 15 mg L^{-1}, (f) 25 mg L^{-1} onto V_xG_y heterojunctions at pH value of 7.

Notes and references

1 S.S. Xue, D.L. He, X.C. Hu, Y.Q. Cao, J.L. Ge, S.X. Liu, *J. Polym. Eng.*, 2023, **43**, 594.
2 J.Y. Li, X. Yu, Y. Zhu, X.H. Fu, Y.M. Zhang, *J. Alloy Compd.*, 2021, **850**, 156778.
3 M. Madi, M. Tahir, Z.Y. Zakaria, *J. CO_2 Util.*, 2022, **65**, 102238.